Dependence of Climate Sensitivity on the Given Distribution of Relative Humidity

Stella Bourdin[1,1], Lukas Kluft[2,2], and Bjorn Stevens[2,2]

[1]LSCE/IPSL, Université Paris-Saclay
[2]Max Planck Institute for Meteorology

November 30, 2022

Abstract

We study how the vertical distribution of relative humidity (RH) affects climate sensitivity, even if it remains unchanged with warming. Using a radiative-convective equilibrium model, we show that the climate sensitivity depends on the shape of a fixed vertical distribution of humidity, tending to be higher for atmospheres with higher humidity. We interpret these effects in terms of the effective emission height of water vapor. Differences in the vertical distribution of RH are shown to explain a large part of the 0 to 30% differences in clear-sky sensitivity seen in climate and storm-resolving models. The results imply that convective aggregation reduces climate sensitivity, even when the degree of aggregation does not change with warming. Combining our findings with relative humidity trends in reanalysis data shows a tendency toward Earth becoming more sensitive to forcing over time. These trends and their height variation merit further study.

Dependence of Climate Sensitivity on the Given Distribution of Relative Humidity

S. Bourdin[1,2], **L. Kluft**[1,3,4], **B. Stevens** [1]

[1]Max-Planck Institute for Meteorology, Hamburg, Germany
[2]Laboratoire des Sciences du Climat et de lEnvironnement, LSCE/IPSL, CEA-CNRS-UVSQ, Universit Paris-Saclay, Gif-sur-Yvette, F-91191, France
[3]International Max Planck Research School on Earth System Modelling
[4]Universitt Hamburg, Faculty of Mathematics, Informatics and Natural Sciences, Department of Earth Sciences, Meteorological Institute, Hamburg, Germany

Key Points:

- Climate sensitivity is sensitive to the assumed distribution of relative humidity.
- Different relative humidity profiles explain clear-sky climate sensitivity spread among models.
- Tropical relative humidity trend in reanalyses yields an increase in climate sensitivity.

Corresponding author: Stella Bourdin, stella.bourdin@lsce.ipsl.fr

This article has been accepted for publication and undergone full peer review but has not been through the copyediting, typesetting, pagination and proofreading process, which may lead to differences between this version and the Version of Record. Please cite this article as doi: 10.1029/2021GL092462.

Abstract

We study how the vertical distribution of relative humidity (RH) affects climate sensitivity, even if it remains unchanged with warming. Using a radiative-convective equilibrium model, we show that the climate sensitivity depends on the shape of a fixed vertical distribution of humidity, tending to be higher for atmospheres with higher humidity. We interpret these effects in terms of the effective emission height of water vapor. Differences in the vertical distribution of RH are shown to explain a large part of the 10 % to 30 % differences in clear-sky sensitivity seen in climate and storm-resolving models. The results imply that convective aggregation reduces climate sensitivity, even when the degree of aggregation does not change with warming. Combining our findings with relative humidity trends in reanalysis data shows a tendency toward Earth becoming more sensitive to forcing over time. These trends and their height variation merit further study.

Plain Language Summary

Equilibrium Climate Sensitivity is the change in surface temperature in response to a doubling of atmospheric CO_2. We study how the assumed vertical distribution of relative humidity affects this sensitivity. Theoretical considerations show that the more moist an atmosphere is, the more it warms as a response to an increase in CO_2. Adding water vapor to the lower troposphere has the counter effect, lowering the sensitivity. We emphasize the importance of climate simulations taking humidity into account, as it is largely responsible for the difference in projections among models without clouds. We note surprising trends in humidity – with substantial drying of the lower troposphere over the ocean – in the last four decades as reported by two reanalyses of meteorological observations. Subject to the accuracy of these reconstructions, there appears to be a change with less moistening than expected, but with moistening/drying profiles which will condition Earth to become more sensitive to forcing over time. We stress the need for a study of observations to more critically evaluate these trends, and know better what models should aim for.

1 Introduction

The clear-sky response to an increase in greenhouse gases is a pillar of our understanding of global warming (Manabe & Wetherald, 1967; Charney et al., 1979). It is generally believed that this response is better described by an atmosphere whose relative, rather than absolute, humidity remains constant with warming.

The distinction is crucial because in an atmosphere where the relative humidity (RH) is fixed, the response of surface temperature to radiative forcing (e.g., from changing CO_2), is roughly twice as large as would be the case should absolute humidity be fixed. In an influential review of these matters, Held and Soden (2000) presented theoretical arguments and evidence from modelling in support of a constant relative humidity. At the time of their review, observations were insufficient to test this hypothesis, but Held and Soden concluded that "10 years may be adequate, and 20 years will very likely be sufficient, [...] to convincingly confirm or refute the predictions". It is now twenty years later.

Taken at face value, two reanalyses of meteorological observations support this point of view, albeit less convincingly than we anticipated. This is shown in Fig. 1, where above 600 hPa RH is increasing with warming, at a rate of 1 %/decade to 4 %/decade. Rather than attempting to establish the reliability of the trends – a task for which we lack expertise – our aim is to estimate their implication for how Earth's equilibrium climate sensitivity may be changing. How does a moister upper, or drier lower, troposphere make Earth more or less sensitive to forcing? Posing this question raises even more basic ques-

tions. For instance, to what extent does the given profile of RH matter for the clear-sky climate sensitivity, even if it remains constant with warming?

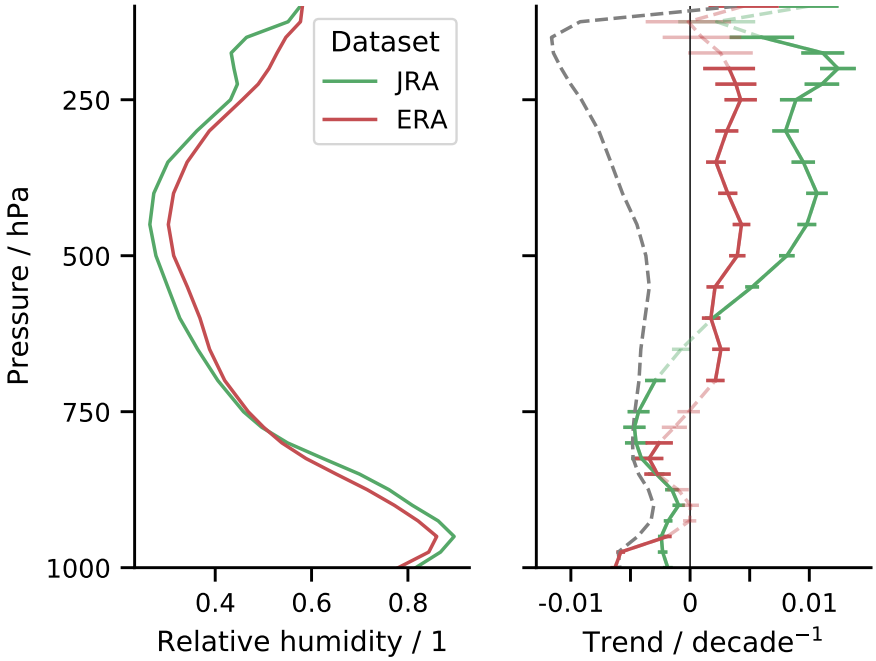

Figure 1. Mean profile (left) and linear trend over 40 years (solid, right) for ERA5 and JRA-55 reanalysis data. Error bars show the 95% confidence interval for the gradient estimation. Lighter and dashed parts indicate levels for which the null hypothesis of the trend being zero has not been rejected (p-value $>$ 0.01). The grey dashed line corresponds to what would be the trend in relative humidity for a constant absolute humidity considering ERA5 tropical temperature trend. Details about the trend analysis are given in SI.

If the water vapor pressure, e, changes to keep RH constant with warming, then the fractional vapor pressure change is given by the Clausius-Clapeyron equation, as

$$\frac{\delta e}{e} = \frac{\ell_\mathrm{v}}{R_\mathrm{v} T^2} \delta T, \tag{1}$$

with ℓ_v the vaporization enthalpy, R_v the water vapor gas constant, and T temperature. To the extent the radiative response to an increase in water vapor depends on its fractional change, as for instance is the case for well mixed greenhouse gases (Huang et al., 2016), Eq. (1) predicts that this response – and hence the water vapor feedback – should be independent of RH. Support for this point of view is provided by observations and analyses that show outgoing long-wave radiation (OLR) varying linearly with T in a manner that is independent of RH (Koll & Cronin, 2018; Zhang et al., 2020). These same studies show, however, that the robustness of this relationship is mostly a feature of a colder atmosphere. In the tropics, where continuum emission by water vapor in the 800 cm^{-1} to 1200 cm^{-1} spectral (window) region becomes more important, RH begins to color the relationship between OLR and T. The tropics cover a substantial portion of the Earth, which raises the question as to whether a sensitivity of the water vapor feedback to the given profile of RH might in part explain differences (15 %, one sigma) in clear-sky feedbacks across climate models (Soden & Held, 2006; Vial et al., 2013), differences that are even larger across simulations designed to isolate the response of the tropical atmosphere

to warming (Medeiros et al., 2008; Becker & Wing, 2020). Questions such as these have not been the topic of much study. Past work has focused on cloud changes (Stevens et al., 2016; Sherwood et al., 2020), to a degree that can give the impression that clouds alone stand in the way of a meaningful quantification of how surface temperatures, T, respond to radiative forcing. Exceptional is the study by Po-Chedley et al. (2018), who argue that changes in RH in the southern-hemisphere extra-tropics are a large source of model spread; here we emphasize how and why such effects are also substantial in the tropics.

The idea that the climate response is sensitive to the particular distribution of relative humidity being held fixed, can be thought of as a form of state dependence. Perhaps for the reasons given above, most studies addressing this issue adopt a conceptual framework that only admit surface temperature as a state variable (Meraner et al., 2013; Knutti et al., 2017). So long as RH does not vanish, it plays no role.

In the present article we report on our investigation of the influence of RH on climate sensitivity using a 1D radiative-convective equilibrium (RCE) model, and highlight a phenomenon we call humidity–dependence. Such a model is attractive for our purposes because it captures (often with surprising fidelity) the behavior of more elaborated descriptions of the climate system in a physically transparent manner. In §2 we describe the model and methods. In §3 we compute the relative impact of a perturbation in the profile at different levels, as a function of RH. In §4 we simulate less idealized profiles of RH to understand and better quantify their effect on on the spread in clear-sky climate sensitivity produced by more elaborated models. In §5 we return to the trends in the reanalysis RH to quantify their implications for our understanding of the clear-sky climate sensitivity. We conclude in §6.

2 Model & Methods

Calculations were performed using the 1D-RCE model konrad (Kluft et al., 2019; Dacie et al., 2019). We adopt a configuration that uses the RRTMG radiative scheme (Mlawer et al., 1997) and a hard convective adjustment (Dacie, 2020) following the moist adiabatic lapse rate. Only clear-sky calculations are performed. In a subset of calculations discussed at the beginning of §3, we also used a uniform lapse rate. We used 500 pressure levels between 1000 hPa and 0.5 hPa. Following the prescription of the Radiative Convective Equilibrium Model Intercomparison Project, RCEMIP (Wing et al., 2018), the solar constant is set to $551.58\,\mathrm{W\,m^{-2}}$ and the zenith angle to 42.05°, resulting in an insolation of $409.6\,\mathrm{W\,m^{-2}}$. The surface albedo is 0.2. The ozone profile is defined according to RCEMIP guidelines (Wing et al., 2018), with additional coupling to the cold-point tropopause allowing the ozone layer to shift with troposphere deepening (Kluft, 2020). The RH follows a prescribed vertical distribution up to the cold-point above which the specific humidity is kept uniform at its cold-point value. The RH is defined with respect to saturation over water above 0 °C and with respect to saturation over ice below −23 °C. In between, a combination of both is used (ECMWF, 2018).

A *run* is defined by its RH profile. It is composed of two equilibrium computations: (i) a spin-up with a constant surface temperature $T_0 = 300\,\mathrm{K}$, (ii) a new equilibrium after applying a sudden doubling of the CO_2 concentration. In (ii) the surface has no longer a fixed temperature but a fixed enthalpy sink, whose value is the top of the atmosphere radiative imbalance at the end of the spin-up, as Kluft (2020) argues to be best practice. The Equilibrium Climate Sensitivity, $\mathcal{S}$ of our model is defined as the difference between the second equilibrium surface temperature and T_0.

In §3, we discuss *perturbation runs*. In these, the tropospheric RH profile is uniform except for a 600 m thick layer, where the RH is increased or decreased (the perturbation). A perturbation run is thus defined by a base RH, a perturbation pressure, and

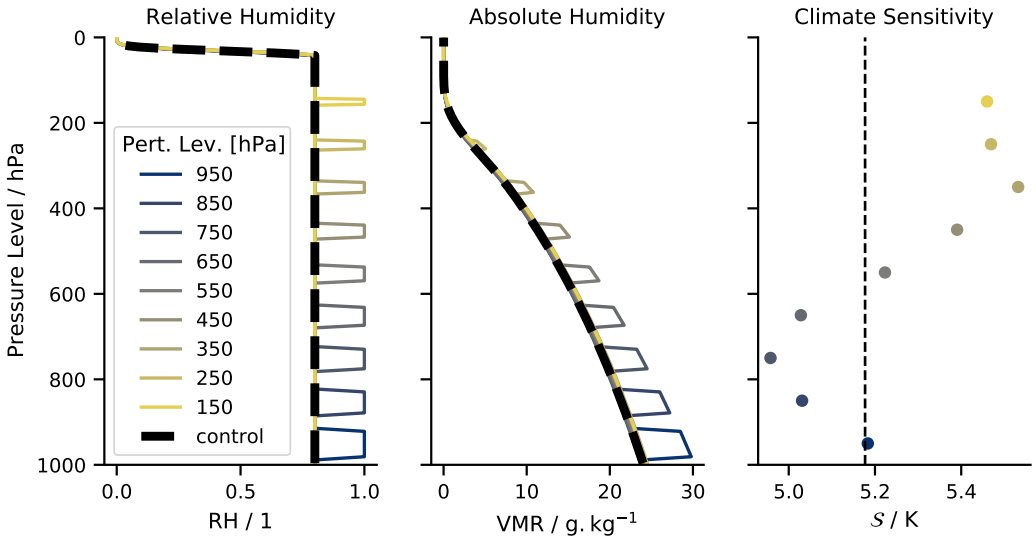

Figure 2. Illustration of the *perturbation runs* method. The control run, with a base RH of 0.8, is shown in dashed black. Each color corresponds to a run with a perturbation $\delta_{RH} = 0.2$ at a different level. The two left panels show the relative and absolute humidity profiles. The right panel shows $\mathcal{S}$ for each *perturbation run* as a function of perturbation pressure alongside the value of $\mathcal{S}$ for the control run (dashed vertical line).

a perturbation intensity δ_{RH}. The corresponding 'run' without perturbation is called a *control run*. This is illustrated in Fig. 2. Arithmetic changes in RH are adopted, as they correspond to geometric changes in absolute humidity, to which (as a first approximation) the radiative response is proportional, irrespective of the base RH.

As a measure of the impact of a perturbation, we define the amplification factor a as the ratio of the $\mathcal{S}$ in the perturbation run, $\mathcal{S}_{\mathrm{p}}$, to the $\mathcal{S}$ in the corresponding control run, $\mathcal{S}_{\mathrm{c}}$:

$$a = \frac{\mathcal{S}_{\mathrm{p}}}{\mathcal{S}_{\mathrm{c}}} - 1. \tag{2}$$

In reanalysis data, see Fig. 1, the RH profiles peak in the boundary layer and in the upper-troposphere and show a distinct minimum in the mid-troposphere. For this reason, we call such a profile *C-shaped*. In order to simulate a C-shaped RH profile, we developed the following piecewise model, in pressure coordinates (shown in Fig. 4):

- Linear in the boundary layer, from the surface to the lower-tropospheric peak (low point);
- Quadratic in the mid-troposphere, defined by 3 points: the two peaks and the humidity at 500 hPa (mid point);
- Linear above the upper-tropospheric peak, defined by the upper-tropospheric peak (top point) and the cold-point (which is more strongly coupled to T than p).

The advantages of such an RH profile is that it is defined by only 5 points, corresponding to parameters that are straightforward to interpret, and it catches the main feature of a realistic profile better than a uniform profile. Moreover, these parameters give us enough degrees of liberty to fit well AMIP and RCEMIP data, as detailed in §4.

3 Humidity–Dependence of $\mathcal{S}$

To understand how $\mathcal{S}$ varies with mean RH, we first perform runs with different uniform tropospheric RH profiles, both for the case of uniform and moist adiabatic lapse rates. Values of $\mathcal{S}$ for these runs are plotted in Fig. 3 (top panel). We find a robust increase in $\mathcal{S}$ with a moister troposphere. We decomposed $\mathcal{S}$ into contributions from the forcing and the feedback following Gregory et al. (2004). This shows that changes in $\mathcal{S}$ arise from changes in feedback as the forcing tends to be much smaller and of the opposite sign.

Let us use the effective emission height concept for the interpretation of our calculations. Let Φ_e be Earth's infrared irradiance at the top of the atmosphere. It can be associated with radiant power emitted by a black body at a temperature, T_e, such that $\Phi_\mathrm{e} = \sigma T_\mathrm{e}^4$, where σ is the Stefan-Boltzmann constant. We define the *effective emission height* to be the altitude z_e such that $T(z_\mathrm{e}) = T_\mathrm{e}$. These ideas can be generalized to allow for spectrally specific effective emission heights, which we denote $z_{\mathrm{e},\lambda}$, as done by Seeley and Jeevanjee (2021).

To help understand the water vapor feedback, we first apply this concept to a case with a uniform lapse rate, $\mathrm{d}T/\mathrm{d}z = -\Gamma$, and grey radiation characterized by a single emission height. If an initial (positive) perturbation in CO_2 causes an increase in the emission height $\delta z_{\mathrm{e,i}} > 0$, the troposphere (and surface) warms until $T(\delta z_{\mathrm{e,i}}) = T_\mathrm{e}$ to maintain Φ_e. As a reaction to this warming, if RH is to remain fixed, the absolute humidity must increases following Eq. (1). The fractional increase in water vapor partial pressure $\delta e/e$ will in turn lead to a further change in z_e, which must be balanced by further warming, increasing humidity, and so on. $\mathcal{S}$, is the sum of the response from the initial forcing, plus this water vapor feedback.

The increase in $\mathcal{S}$ with RH (Fig. 3) calls into question the line of reasoning (§1) leading to the expectation that $\mathcal{S}$ is independent of RH. This may be indicative of continuum emission and absorption by water vapor in the window ($800\,\mathrm{cm}^{-1}$ to $1200\,\mathrm{cm}^{-1}$) region, which increases non-linearly with absolute humidity (Koll & Cronin, 2018). This would give rise to a stronger humidity-dependence of $\mathcal{S}$ at high temperatures. We thus repeat our calculations at lower values of T_0, at which the effect of the water vapor continuum is negligible. Reducing the working temperature progressively reduces the sensitivity to RH – at $T_0 = 288\,\mathrm{K}$ $\mathcal{S}$ increases by only 25 % as RH increases from 0.1 to 0.9 – consistent with the hypothesis that the unexpected behavior does indeed stem from the effect of continuum emission in the window region.

The case of the moist adiabat (orange points and matrix in Fig. 3) introduces additional complications. A property of the moist adiabat is that the lapse rate monotonically decreases with temperature. This gives rise to three effects: (i) as the atmosphere warms the mean lapse rate becomes smaller (lapse-rate feedback); (ii) for the same surface temperature and mean lapse rate, the moist adiabatic lapse rate is associated with a temperature profile that is everywhere warmer than for the uniform lapse rate; (iii) the lapse-rate is less than the mean in the warmer, lower, troposphere but greater in the colder, upper, troposphere. The first effect gives rise to a negative feedback with warming (smaller $\mathcal{S}$) as it implies that the temperature at the emission height warms more rapidly than at the surface. The second effect gives rise to a positive feedback (larger $\mathcal{S}$) because a warmer atmosphere will (for the same RH) have a larger absolute humidity. The third effect implies a more bottom heavy humidity profile, which would suggest a slight reduction in $\mathcal{S}$.

At low absolute humidities the negative lapse-rate feedback dominates. This explains why in the upper panel of Fig. 3, for $RH \leq 0.75$, runs with a moist-adiabatic lapse rate have a substantially smaller $\mathcal{S}$. This difference becomes even more pronounced (as expected) if one uses the integrated water vapor (IWV) as the control variable. For

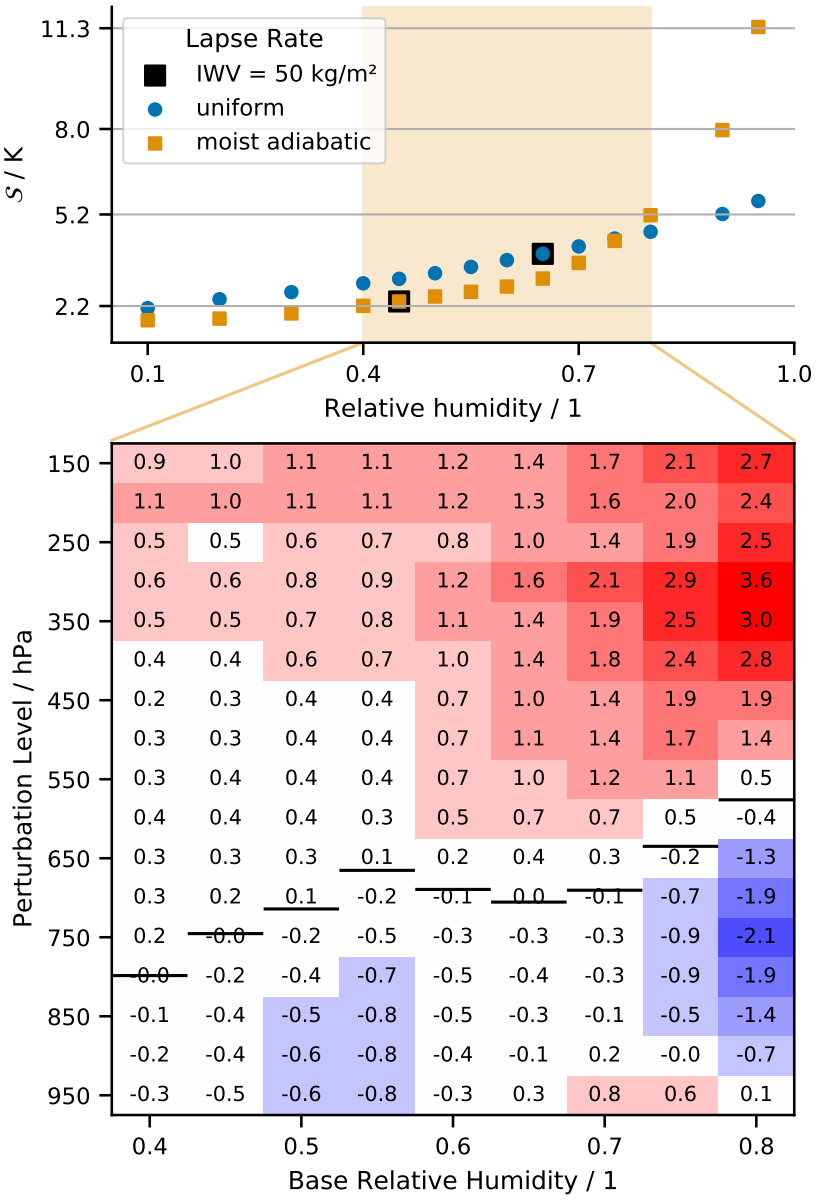

Figure 3. (Upper panel) $\mathcal{S}$ for different uniform tropospheric RH, and for experiments with a uniform tropospheric lapse rate of $6.5\,\mathrm{K\,km^{-1}}$ or with a moist adiabatic lapse rate. Black squared points correspond to experiments were integrated water vapor (IWV) was the closest to $50\,\mathrm{kg\,m^{-2}}$. (Lower panel) Amplification factor a (in percent) for 0.1 RH perturbation for different humidities and different perturbation levels. Blue and red colors for changes larger than 0.5 % in magnitude are indicative of the value's range. Black lines represent the mid-tropospheric level at which a changes sign.

high humidities the second effect dominates. This occurs because for the chosen value of T_0 the atmospheric window looses its transparency (Koll & Cronin, 2018), which is a self-amplifying effect that explains the sharp increase in $\mathcal{S}$. To test our explanation we performed additional calculations with a smaller T_0. As the above argument would anticipate, this reduces the sensitivity to RH (see Fig. S3 in the SI), a result that is also consistent with a $\partial_{T_0}\mathcal{S}$ decreasing with T_0, e.g., as shown by Meraner et al. (2013). Finally, calculations (not shown) that adopt a constant moist adiabatic lapse rate (which cannot change with warming) also have a slightly reduced $\mathcal{S}$ as compared to calculations adopting a uniform lapse rate for the same value of IWV. In this case, there is no lapse-rate feedback and the IWV is the same. This supports our interpretation of the third effect, whereby the shape of the humidity profile also influences $\mathcal{S}$.

To assess how the shape of the RH profile influences $\mathcal{S}$ we perform perturbation runs as described in §2 (see also Fig. 2). Perturbation runs are performed with $\delta_{\mathsf{RH}} = -0.1, 0.1, 0.2$. From these the amplification factor, a per Eq. 2, is related to δ_{RH} through linear regression. Fig. 3 plots a from its regressed slope multiplied by $\delta_{\mathsf{RH}} = 0.1$. Values are calculated for RH perturbations applied every 50 hPa to an otherwise constant RH profile. This sequence of height varying perturbation runs is computed for $0.4 \leq \mathrm{RH} \leq 0.8$. The impact of a positive RH perturbation is small, but discernibly positive (increasing $\mathcal{S}$) in the upper troposphere, and negative (decreasing $\mathcal{S}$) in the lower troposphere. Simulations where the perturbations are fixed relative to the profile of T – which in the mid and upper troposphere is, following Romps (2014), likely to be a more realistic representation of RH – lead to weaker changes in $\mathcal{S}$, but imply a similar sensitivity to shape. Perturbations at lower values of p (equivalently lower T) lead to larger increases in $\mathcal{S}$. In every case, the higher the base RH, the stronger is the sensitivity to the humidity perturbation. Moreover, the level of sign change rises with base RH.

The perturbation runs are consistent with our earlier discussion, but not especially intuitive. To understand them, and test their robustness, we performed line-by-line radiative transfer using the ARTS model (Buehler et al., 2018), the results of which are provided graphically in the SI (Fig. S2). We find two opposing effects. In spectral regions where $z_{\mathrm{e},\lambda}$ is near the height of the RH perturbation, the change in $z_{\mathrm{e},\lambda}$ as water-vapor adjusts to warming is lessened. It is as if the fixed perturbation height helps anchor $z_{\mathrm{e},\lambda}$. In spectral regions where the effective emission height is well below the RH perturbation, the change in $z_{\mathrm{e},\lambda}$ as water-vapor adjusts to warming is heightened – increasing the strength of the water vapor feedback. The first (damping) effect explains the reduction in $\mathcal{S}$ associated with RH perturbations in the lower troposphere. It is also apparent at strongly absorbing wave numbers (rotational and ro-vibrational bands) for the perturbations in the upper troposphere. But for the latter case this reduction is more than offset by the second (amplifying) effect whereby the perturbation in the upper atmosphere increases the changes in $z_{\mathrm{e},\lambda}$ in parts of the window-region where CO_2 does not dominate.

We call *humidity–dependence* the fact that the climate sensitivity depends on the relative humidity. Not only does the sensitivity depend on the overall humidity, or IWV, but also on the distribution of humidity, that is the shape of the RH profile.

4 Implications for Model-Based Estimates of ECS

Given the non-linearity of these effects, generalization is not automatic. Here we check whether results of the previous section can also be identified for less idealized perturbations to RH profiles more similar to those observed and simulated by climate models. For this purpose we use C-shaped RH profiles as defined in §2. To reduce their degrees of liberty we additionally fix the low point to 925 hPa and set the slopes below the low point, and above the high point, to $2.0 \times 10^{-5}\,\mathrm{Pa}^{-1}$ and $-5.8 \times 10^{-5}\,\mathrm{Pa}^{-1}$ respectively. These values are the mean of the parameters when fitting to RCEMIP profiles

(see following paragraphs). We additionally set the RH at the cold-point to be half its peak (upper-troposphere) value, the level of this cold-point being computed by konrad. Calculations (runs) were then performed to quantify the impact of changing the remaining parameters: Starting from a 0.7/0.4/0.85 (top/mid/low) profile, we: (i) shifted the whole profile; (ii) changed only the RH at the top of the atmosphere; (iii) changed only the humidity at 500 hPa; (iv) changed only the humidity in the lower atmosphere. Humidity profiles and resulting changes in $\mathcal{S}$ are presented in Fig. 4. Qualitatively the response to these perturbations agrees well with what was learned from the response to more idealized perturbations: (i & ii) $\mathcal{S}$ increases with an increase in the upper tropospheric RH, also when this is part of a general moistening; (iv) $\mathcal{S}$ decreases if RH increases are confined to the lower troposphere; and (iii) increases in RH in the middle troposphere lead to little change in $\mathcal{S}$ until a critical RH (associated with the closing of the window) is reached, at which point $\mathcal{S}$ begins to increases markedly. The same set of experiments have been performed with a C-shaped profile invariant in T in the upper-troposphere, to find very similar results (not shown).

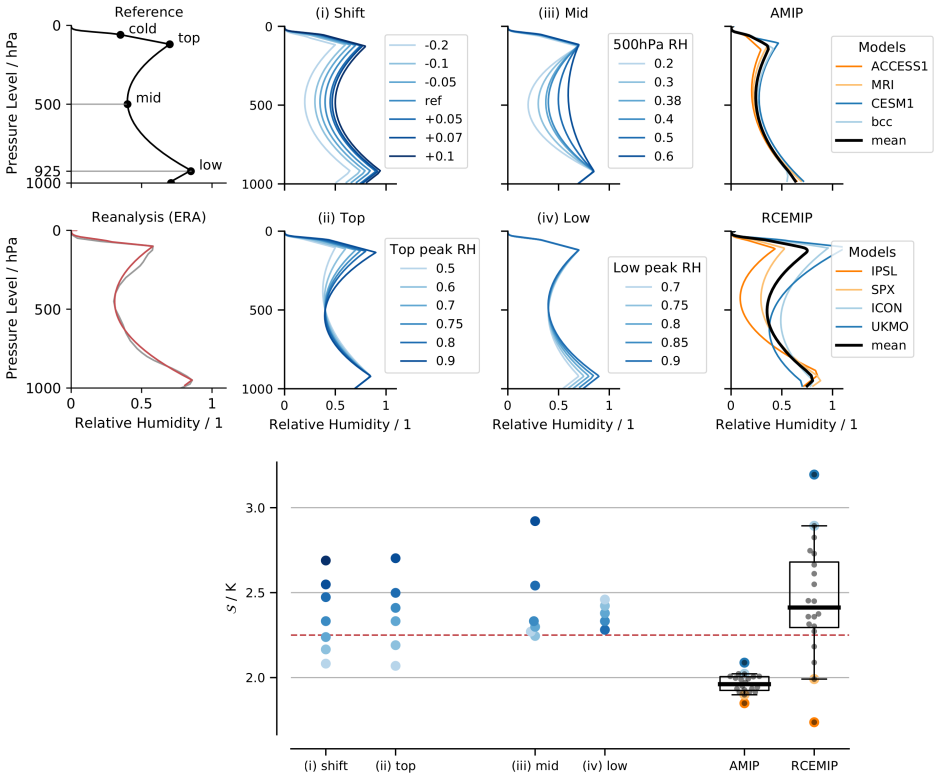

Figure 4. (Upper two rows) C-shaped RH profiles: Reference 0.7/0.4/0.85 (top/mid/low) profile (top-left); ERA5 profile as computed for §5 (grey), and corresponding C-shaped fit (red) (bottom-left). Four central panels correspond to the idealized experiments described in the first paragraph of §4. Two right-most panels display the mean and extreme profiles of the AMIP (top-right) and RCEMIP (bottom-right) datasets. (Lower panel) $\mathcal{S}$ for the idealized experiments and for the experiments with a profile fitted to the AMIP or RCEMIP ensembles. Boxplots' whiskers are set to display the 5th and 95th percentiles. On this graph and for statistics, only one point per model "family" (i.e. issued by the same institute) is used, corresponding to the average of all this family's models. Red dashed line correspond to the $\mathcal{S}$ computed with ERA5 C-shaped fit RH profile above.

In a second step, we performed runs with RH profiles set to fit RCEMIP simulations using storm-resolving and general circulation models (Except for UKMO-CASIM whose humidity profile led to a runaway) on large domains with an SST of 300 K (Wing et al., 2020) and CMIP5 AMIP ensembles. The fit is done by retrieving the pressure and humidity of the five points defining our C-shaped profile. In particular, the low and top points coincide with the local maxima and the cold-point pressure is retrieved from the temperature profile. The mid point remains fixed at 500 hPa and the surface is taken as the lowest point available. This enables us to assess the effect of the humidity profile alone, all other things being equal.

With RCEMIP RH profiles, we find a $\pm 26\%$ variation around the mean $\mathcal{S}$ value. The spread in feedback is $-1.25\,\mathrm{W\,m^{-2}\,K^{-1}}$ to $-3\,\mathrm{W\,m^{-2}\,K^{-1}}$, slightly smaller but comparable to what is found by Becker and Wing (2020). We thus explain the surprisingly large spread in clear-sky sensitivity in RCEMIP as being in large part a response to different RH profiles simulated by the models. Both differences in the IWV and the shape of the profiles contribute to the spread, the latter more so, as is also evident by comparing sensitivities calculated using ICON versus the UKMO RH profiles. To the extent that the inter-model spread in RH to different degrees of convective self-aggregation, as claimed by Becker and Wing (2020), our work suggests that different degrees of convective self-aggregation can influence the climate sensitivity, even if the convective self-aggregation does not change with warming.

From CMIP5 AMIP output, we retrieved mean profiles over the tropical oceans (equatorward of 30°) averaged over the entire simulated period. As compared to RCEMIP RH profiles, those from the AMIP simulations are on average dryer, and thereby associated with a smaller $\mathcal{S}$. The drier AMIP profiles are indicative of large-scale circulations driven by differences in surface temperatures, i.e., Hadley and Walker cells which give rise to the dry tropics. The AMIP simulations differ less in their humidity profiles and likewise show less spread in $\mathcal{S}$, but even so differences approaching 10 % are evident

Given observations of the RH profiles in the atmosphere, it should be possible to correct model estimates of climate sensitivity using calculations such as ours. From a comparison of Fig. 1 and Fig. 4, we note that the RCE models tend to be moister than the observations, the AMIP simulations are drier. Fitting the C-shaped humidity profile to the observations yields an $\mathcal{S}$ of about 2.25 K; this is smaller than that of most RCE models, but larger than for the AMIP models. Likewise, ECS estimates in early calculations following the RH humidity profile used by Manabe and Wetherald (1967), would, due to an unrealistically dry upper atmosphere, be biased too low. However, for the lower humidities and temperatures used in that study, the fixed lapse assumption actually over compensates, leading to a larger sensitivity as seen in Kluft et al. (2019). This, along with the upper panel of Fig. 3, is illustrative of how the lapse rate feedback depends on the base state RH.

5 Impact of RH Trends in Reanalysis Data

Based on the above analysis we return to our initial question, which is how to interpret RH trends in the reanalysis products. The profiles presented in Fig. 1 are from the ERA5 (Hersbach et al., 2020), and the JRA-55 (Kobayashi et al., 2015) reanalyses of the past forty years (1979-2019) of meteorological observations. Relative and absolute humidity, as well as temparature, are averaged over tropical oceans (equatorward of 30°). Trends regressed from monthly data are significant at several levels and consistent across both reanalyses. They are also evident in the difference between the mean profile in the first and last decade (not shown). We were surprised that RH at low levels was robustly decreasing – something that merits further investigation – even if averaged over height $\delta RH \approx 0$. Our analysis does not tell us how strongly these trends influence the expected warming over the past forty years, but it does tell us that the pat-

tern of change, with moistening aloft and drying in the lower middle troposphere is conditioning the climate system toward greater sensitivity.

6 Conclusions

The response of the atmosphere to radiative forcing as a function of the assumed profile of relative humidity (RH) is explored using a one-dimensional radiative-convective equilibrium model. For profiles chosen to sample the range produced by state of the art climate and storm-resolving models run under idealized conditions, the calculated equilibrium climate sensitivity of our model ($\mathcal{S}$) varies between 2 K to 3 K, depending on the RH profile, highlighting a humidity–dependence of the climate sensitivity: Moister atmospheres were shown to have a larger $\mathcal{S}$, increasingly so with warmer temperature, consistent with understanding of how water vapor influences the transmissivity of the atmospheric window (Nakajima et al., 1992; Koll & Cronin, 2018; Seeley & Jeevanjee, 2021). $\mathcal{S}$ is further shown to increase with increasing humidity in the upper troposphere, but decreases with increases in humidity in the lower mid-troposphere.

The use of a simple physical model, konrad, makes it easier to understand the basic physics determining the outcome of our calculations. For instance, with the chosen framework it is possible to show how the the lapse rate's influence on the total amount and vertical distribution of humidity for a given profile of RH influences $\mathcal{S}$. We could also investigate how $\mathcal{S}$ depends on the shape of the RH profile, which expresses competing effects, whereby perturbations to the humidity can both reduce or increase the change in the emission height associated with changes in absolute humidity to maintain a constant relative humidity with warming. The former effect dominates when the humidity perturbation is near the emission height resulting in a slight reduction in $\mathcal{S}$ for bottom heavy humidity profiles.

Our work emphasizes the importance of realistically representing the relative humidity profile when calculating climate sensitivity. Models that are too humid, particularly in the mid- and upper-troposphere will have larger sensitivities, an effect which will amplify with increased warming. Convective self-aggregation modifies the mean relative humidity profile, thereby reducing ECS, even if the degree of convective aggregation itself does not change with warming. In this context, our study also encourages the use of RH as metric of the fidelity of the moist physics in climate models. To the extent climate models are unable to realistically represent the observed distribution of RH, our methods may make it possible to estimate the quantitative effect of these biases.

Humidity profiles over tropical oceans as represented in reanalysis products, tend to be moister than those produced by models forced with observed SSTs, implying a larger clear-sky sensitivity. Three dimensional radiative convective equilibrium models, which are more physical – but less constrained by large-scale sea-surface temperature gradients – tend to be more humid, but also have more divergent humidity profiles.

Surprisingly large changes in RH are reported by the reanalysis products over the last forty years, changes which our calculations suggest will condition the climate system to be more sensitive to forcing in the future. This finding adds an additional dimension to Knutti and Rugenstein's (2015) statement that the feedback parameter is not constant, and that non-linearity in the system may be important when assessing Earth's equilibrium climate sensitivity. The surprising trends in the reanalysis humidity products, particularly the drying in the tropical lower troposphere, reminds us of Held and Soden's plea to be attentive to this issue, and merits the renewed attention of experts.

Acknowledgments

The research is supported by public funding to the Max Planck Society. S.B. also benefited from the French state aid managed by the ANR under the "Investissements d'avenir"

programme with the reference ANR-11-IDEX-0004 - 17-EURE-0006. B.S. and L.K. acknowledge support from the European Union's Horizon 2020 Research and Innovation Programme under grant agreement No. 820829 (CONSTRAIN Project). We thank Tobias Becker, Sally Dacie, Didier Paillard, Maria Rugenstein and Catherine Stauffer for helpful scholar discussion concerning this study, and Hauke Schmidt's GCC group at MPI-M for advice and feedback. We are also grateful to Sbastien Fromang and Theresa Lang for their review of an earlier version of this manuscript, as well as the stimulating and thoughtful comments of Nadir Jeevanjee and an anonymous reviewer, which stimulated a deeper understanding of our results.

- Primary data including simulation scripts and code for reproducing the figures are available on Zenodo through `https://doi.org/10.5281/zenodo.4559581`.
- konradv0.8.1 is available at `github.com/atmtools/konrad`, and latest sources are available at `https://doi.org/10.5281/zenodo.4434837`.
- ERA5 data is available on the Copernicus Climate Change Service Climate Data Store (CDS, `https://cds.climate.copernicus.eu/cdsapp#!/dataset/reanalysis-era5-pressure-levels-monthly-means?tab=overview`).
- JRA-55 data were retrieve from `https://jra.kishou.go.jp/JRA-55/index_en.html`.
- The German Climate Computing Center (DKRZ) hosts the standardized RCEMIP and CMIP5-AMIP output (`https://cera-www.dkrz.de/WDCC/ui/cerasearch/info?site=RCEMIP_DS`).

The authors declare no conflict of interest.

References

Becker, T., & Wing, A. A. (2020). Understanding the extreme spread in climate sensitivity within the radiative-convective equilibrium model intercomparison project. *Journal of Advances in Modeling Earth Systems*, *12*(10). doi: 10.1029/2020MS002165

Buehler, S. A., Mendrok, J., Eriksson, P., Perrin, A., Larsson, R., & Lemke, O. (2018). ARTS, the atmospheric radiative transfer simulator — version 2.2, the planetary toolbox edition. *Geoscientific Model Development*, *11*(4), 1537–1556. doi: 10.5194/gmd-11-1537-2018

Charney, J. G., Arakawa, A., Baker, D. J., Bolin, B., Dickinson, R. E., Goody, R. M., ... Wunsch, C. I. (1979). *Carbon dioxide and climate: a scientific assessment*. National Academy of Sciences, Washington, DC.

Dacie, S. (2020). *Using simple models to understand changes in the tropical mean atmosphere under warming* (Unpublished doctoral dissertation). University of Hamburg, Hamburg.

Dacie, S., Kluft, L., Schmidt, H., Stevens, B., Buehler, S. A., Nowack, P. J., ... Birner, T. (2019). A 1D RCE Study of Factors Affecting the Tropical Tropopause Layer and Surface Climate. *Journal of Climate*, *32*(20), 6769–6782. doi: 10.1175/JCLI-D-18-0778.1

ECMWF. (2018). Part iv : Physical processes. In *Ifs documentation cy45r1.* Author. Retrieved from `https://www.ecmwf.int/node/18714`

Gregory, J. M., Ingram, W. J., Palmer, M. A., Jones, G. S., Stott, P. A., Thorpe, R. B., ... Williams, K. D. (2004). A new method for diagnosing radiative forcing and climate sensitivity. *Geophysical Research Letters*, *31*(3). doi: 10.1029/2003GL018747

Held, I. M., & Soden, B. J. (2000). Water Vapor Feedback and Global Warming. *Annual Review of Energy and the Environment*, *25*(1). doi: 10.1146/annurev.energy.25.1.441

Hersbach, H., Bell, B., Berrisford, P., Hirahara, S., Horányi, A., Muñoz-Sabater, J., ... others (2020). The era5 global reanalysis. *Quarterly Journal of the Royal Meteorological Society*, *146*(730), 1999–2049.

Huang, Y., Tan, X., & Xia, Y. (2016). Inhomogeneous radiative forcing of homogeneous greenhouse gases. *Journal of Geophysical Research: Atmospheres*, *121*(6), 2780–2789. doi: 10.1002/2015JD024569

Kluft, L. (2020). *Benchmark Calculations of the Climate Sensitivity of Radiative-Convective Equilibrium* (Doctoral dissertation, Universitt Hamburg, Hamburg). doi: 10.17617/2.3274272

Kluft, L., Dacie, S., Buehler, S. A., Schmidt, H., & Stevens, B. (2019). Re-examining the first climate models: Climate sensitivity of a modern radiative-convective equilibrium model. *Journal of Climate*, *32*, 8111–8125. doi: 10.1175/JCLI-D-18-0774.1

Knutti, R., & Rugenstein, M. A. A. (2015). Feedbacks, climate sensitivity and the limits of linear models. *Philosophical Transactions of the Royal Society A: Mathematical, Physical and Engineering Sciences*, *373*(2054), 20150146. doi: 10.1098/rsta.2015.0146

Knutti, R., Rugenstein, M. A. A., & Hegerl, G. C. (2017). Beyond equilibrium climate sensitivity. *Nature Geoscience*, *10*(10), 727–736. doi: 10.1038/ngeo3017

Kobayashi, S., Ota, Y., Harada, Y., Ebita, A., Moriya, M., Onoda, H., ... others (2015). The jra-55 reanalysis: General specifications and basic characteristics. *Journal of the Meteorological Society of Japan. Ser. II*, *93*(1), 5–48.

Koll, D. D. B., & Cronin, T. W. (2018). Earths outgoing longwave radiation linear due to H2O greenhouse effect. *Proceedings of the National Academy of Sciences*, *115*(41), 10293–10298. doi: 10.1073/pnas.1809868115

Manabe, S., & Wetherald, R. T. (1967). Thermal Equilibrium of the Atmosphere with a Given Distribution of Relative Humidity. *Journal of the Atmospheric Sciences*, *24*, 241–259. doi: 10.1175/1520-0469(1967)024⟨0241:TEOTAW⟩2.0.CO;2

Medeiros, B., Stevens, B., Held, I. M., Zhao, M., Williamson, D. L., Olson, J. G., & Bretherton, C. S. (2008). Aquaplanets, climate sensitivity, and low clouds. *Journal of Climate*, *21*(19), 4974 – 4991. doi: 10.1175/2008JCLI1995.1

Meraner, K., Mauritsen, T., & Voigt, A. (2013). Robust increase in equilibrium climate sensitivity under global warming. *Geophysical Research Letters*, *40*(22), 5944–5948. doi: 10.1002/2013GL058118

Mlawer, E. J., Taubman, S. J., Brown, P. D., Iacono, M. J., & Clough, S. A. (1997). Radiative transfer for inhomogeneous atmospheres: RRTM, a validated correlated-k model for the longwave. *Journal of Geophysical Research: Atmospheres*, *102*(D14), 16663–16682. doi: 10.1029/97JD00237

Nakajima, S., Hayashi, Y.-Y., & Abe, Y. (1992, December). A Study on the ?Runaway Greenhouse Effect? with a One-Dimensional Radiative?Convective Equilibrium Model. *Journal of Atmospheric Sciences*, *49*(23), 2256–2266. doi: 10.1175/1520-0469(1992)049⟨2256:ASOTGE⟩2.0.CO;2

Po-Chedley, S., Armour, K. C., Bitz, C. M., Zelinka, M. D., Santer, B. D., & Fu, Q. (2018). Sources of Intermodel Spread in the Lapse Rate and Water Vapor Feedbacks. *Journal of Climate*, *31*(8), 3187–3206. doi: 10.1175/JCLI-D-17-0674.1

Romps, D. M. (2014). An analytical model for tropical relative humidity. *Journal of Climate*, *27*(19), 7432–7449.

Seeley, J. T., & Jeevanjee, N. (2021). H_2O windows and CO_2 radiator fins: a clear-sky explanation for the peak in ecs. *Geophysical Research Letters*, *n/a*(n/a), e2020GL089609. Retrieved from `https://agupubs.onlinelibrary.wiley.com/doi/abs/10.1029/2020GL089609` (e2020GL089609 2020GL089609) doi: https://doi.org/10.1029/2020GL089609

Sherwood, S., Webb, M. J., Annan, J. D., Armour, K. C., Forster, P. M., Harg-

reaves, J. C., ... Zelinka, M. D. (2020). An assessment of Earth's climate sensitivity using multiple lines of evidence. *Reviews of Geophysics*. doi: 10.1029/2019RG000678

Soden, B. J., & Held, I. M. (2006). An assessment of climate feedbacks in coupled ocean-atmosphere models. *Journal of Climate*, *19*(14), 3354–3360. doi: 10.1175/JCLI3799.1

Stevens, B., Sherwood, S. C., Bony, S., & Webb, M. J. (2016). Prospects for narrowing bounds on Earth's equilibrium climate sensitivity. *Earth's Future*, *4*(11), 512–522. doi: 10.1002/2016EF000376

Vial, J., Dufresne, J.-L., & Bony, S. (2013). On the interpretation of inter-model spread in CMIP5 climate sensitivity estimates. *Climate Dynamics*, *41*(11), 3339–3362. doi: 10.1007/s00382-013-1725-9

Wing, A. A., Reed, K. A., Satoh, M., Stevens, B., Bony, S., & Ohno, T. (2018). Radiative-convective Equilibrium Model Intercomparison Project. *Geoscientific Model Development*, 793–813.

Wing, A. A., Stauffer, C. L., Becker, T., Reed, K. A., Ahn, M.-S., Arnold, N. P., ... Zhao, M. (2020). Clouds and Convective Self-Aggregation in a Multimodel Ensemble of Radiative-Convective Equilibrium Simulations. *Journal of Advances in Modeling Earth Systems*, *12*(9), e2020MS002138. doi: https://doi.org/10.1029/2020MS002138

Zhang, Y., Jeevanjee, N., & Fueglistaler, S. (2020). Linearity of Outgoing Longwave Radiation: From an Atmospheric Column to Global Climate Models. *Geophysical Research Letters*, *47*(17), e2020GL089235. doi: 10.1029/2020GL089235

Supplementary Information

for *Dependence of Relative Humidity on the Given Distribution of Relative Humidity*

S. BOURDIN, L. KLUFT and B. STEVENS

1 Reanalyses' Relative Humidity Trend Analysis

This document aims at describing more precisely the trend analysis on reanalysis data. It is available as a Jupyter Notebook at https://doi.org/10.5281/zenodo.4423267, along with the necessary data.

Two datasets have been used for this analysis : ERA5 and JRA-55. ERA5 is available on the Climate Data Store (https://cds.climate.copernicus.eu/cdsapp#!/dataset/reanalysis-era5-pressure-levels-monthly-means?tab=overview) and was in our case retrieved from a miror on the IPSL servers because the amount of data necessary was very long to obtain through the CDS API. JRA-55 was retrieve from their FTP server, now unavailable. Other means to access the data are describe on their website : https://jra.kishou.go.jp/JRA-55/index_en.html.

1.1 Data pre-processing

1.1.1 ERA5

ERA5 relative humidity data was available in monthly files containing 6-hourly time step. For each monthly files, using nco, we (1) averaged the data over each month (`ncra $mthfile r_${date}.nc`), (2) extracted the tropical zone between +/- 30° (`ncks -v r -d latitude,-30.0,+30.0 r_${date}.nc r_$[date}.nc`). Then concatenated all the data in one file (`ncrcat r_*.nc r_ERA.nc`). We also retrieve the corresponding land-sea mask (`lsm_ERA.nc`).

A python script was apply to retrieve the mean tropical profile over oceans for each month (Note : We did not apply a weighted average assuming grid cell area differences in this region was negligible.) :

```
from dynamicopy import var_load
import numpy as np
import pickle as pkl
import os

# Load data
f = 'r_ERA.nc'
H = var_load('r', f)
P = var_load('level', f)

f_lsm = 'lsm_ERA.nc'
```

```
lsm = var_load('lsm', f_lsm)
mask = lsm[0] < 0.1
H_masked = H * mask
H_masked[H_masked == 0.0] = np.nan

H_tropical = np.nanmean(np.nanmean(H_masked, -1), -1)

with open('H_tropical.pkl', 'wb') as handle:
    pkl.dump(H_tropical, handle)
```

1.1.2 JRA-55

Monthly JRA-55 data was available on the FTP server, but in GRIB format. It was copied to NetCDF using `cdo -f nc copy $file ${file}.nc`, then all the file were concatenated before cutting the -30°/+30° latitude zone, and the same script was applied to obtain the tropical mean profile.

1.2 Trend computation

The trends are computed using a linear regression, and dismissing the hypothesis that the trend might be zero.

[1]:
```
import pickle as pkl
import numpy as np
from scipy import stats
import matplotlib.pyplot as plt
import seaborn as sns
```

[2]:
```
#Load data
##ERA5
with open("ERA/P_ERA.pkl",'rb' ) as handle :
    P_ERA = pkl.load(handle)
with open("ERA/H_tropical.pkl", "rb") as handle:
    H_trop_ERA = pkl.load(handle)
t_ERA = np.arange(len(H_trop_ERA))/12 + 1979 # Time axis in years
### Cut level above 100hPa
H_trop_ERA = H_trop_ERA[:,P_ERA >= 100]
P_ERA = P_ERA[P_ERA >= 100]
```

[3]:
```
## JRA-55
with open("JRA/P_JRA.pkl",'rb' ) as handle :
    P_JRA = pkl.load(handle)
with open("JRA/H_tropical.pkl", "rb") as handle:
    H_trop_JRA = pkl.load(handle)
t_JRA = np.arange(len(H_trop_JRA))/12 + 1979 # Time axis in years
```

To compute the trend, we use `scipy.stats.linregress` function, whose output is defined as follows in the documentation :

```
    Returns
    -------
    slope : float
        Slope of the regression line.
    intercept : float
        Intercept of the regression line.
    rvalue : float
        Correlation coefficient.
    pvalue : float
        Two-sided p-value for a hypothesis test whose null hypothesis is
        that the slope is zero, using Wald Test with t-distribution of
        the test statistic.
    stderr : float
        Standard error of the estimated gradient.
```

In particular, the "error" or uncertainty refers to the `stderr` which is the standard error for the gradient estimation or 67% confidence interval, and the p-value is computed for a null hypothesis where the slope is zero. We use 0.01 as a discriminating threshold for p-values, but p-values are displayed for you to appreciate.

[4]:
```
# Compute trend
##Function
def compute_linear_trend(time, H) :
    trends, intercepts, p_values, stderrs = [], [], [], []
    for p in range(np.shape(H)[1]) :
        slope, intercept, r, p, stderr = stats.linregress(time, H[:,p])
        trends.append(slope)
        intercepts.append(intercept)
        p_values.append(p)
        stderrs.append(stderr)
    return np.array([trends, intercepts, p_values, stderrs])
```

[5]:
```
## ERA
trends_ERA, intercepts_ERA, pvals_ERA, errs_ERA = compute_linear_trend(t_ERA,␣
 ↪H_trop_ERA)
mtrends_ERA = np.ma.masked_array(trends_ERA, pvals_ERA > 0.01)
```

[6]:
```
## JRA
trends_JRA, intercepts_JRA, pvals_JRA, errs_JRA = compute_linear_trend(t_JRA,␣
 ↪H_trop_JRA)
mtrends_JRA = np.ma.masked_array(trends_JRA, pvals_JRA > 0.01)
```

[7]:
```
[Plotting commands]
```

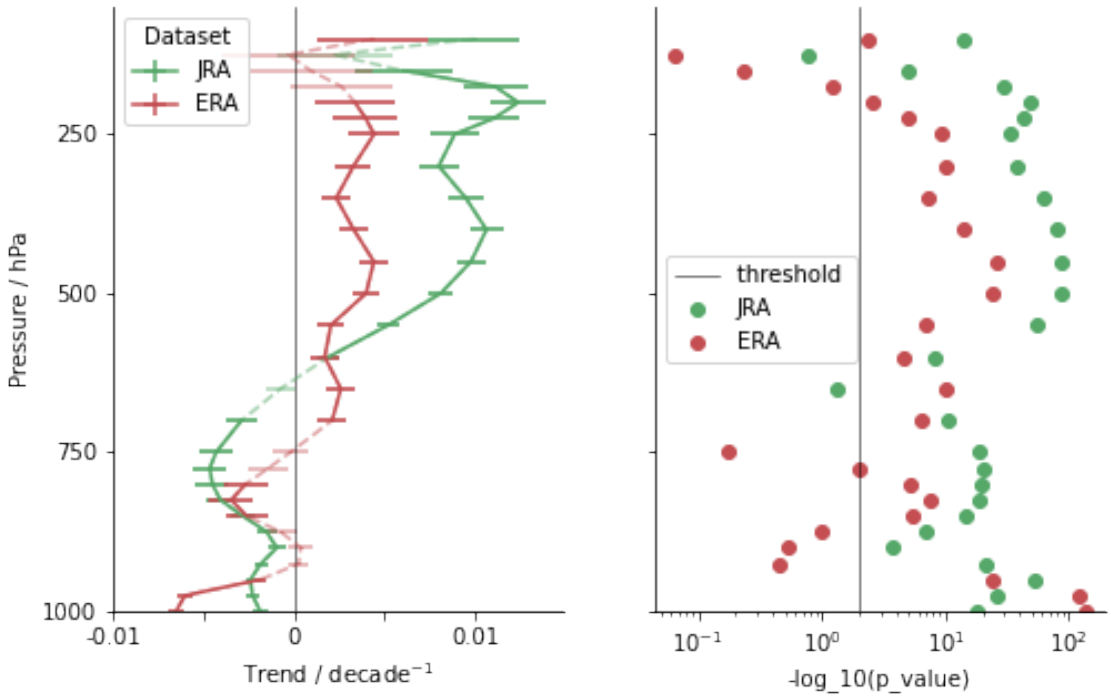

The figure above summarizes our trend analysis : On the left panel is the trend in both reanalysis products, at each levels, with dashed line and transparent points where the p-value > 0.01 does not allow us to conclude that the trend is not zero. Errorbars show 95% confidence interval ($2 \times \sigma$). On the right panel is displayed the logarithm of the p-value for each trend computation, as compared to the threshold.

1.3 Time series

Here we display a few time series to illustrate the trend. Dots indicate the monthly values, solid line the yearly average of these values, and dashed line the linear trend corresponding to what is above.

[8]:
```
def yearly_avg(H) :
    return np.array([np.mean(H[yr*12:(yr+1)*12],0) for yr in range(int(len(H)/
 ↪12))])
H_ERA_yr = yearly_avg(H_trop_ERA)
H_JRA_yr = yearly_avg(H_trop_JRA)
yrs = np.arange(1979, 2020)
```

[9]:
```
[Plotting commands]
```

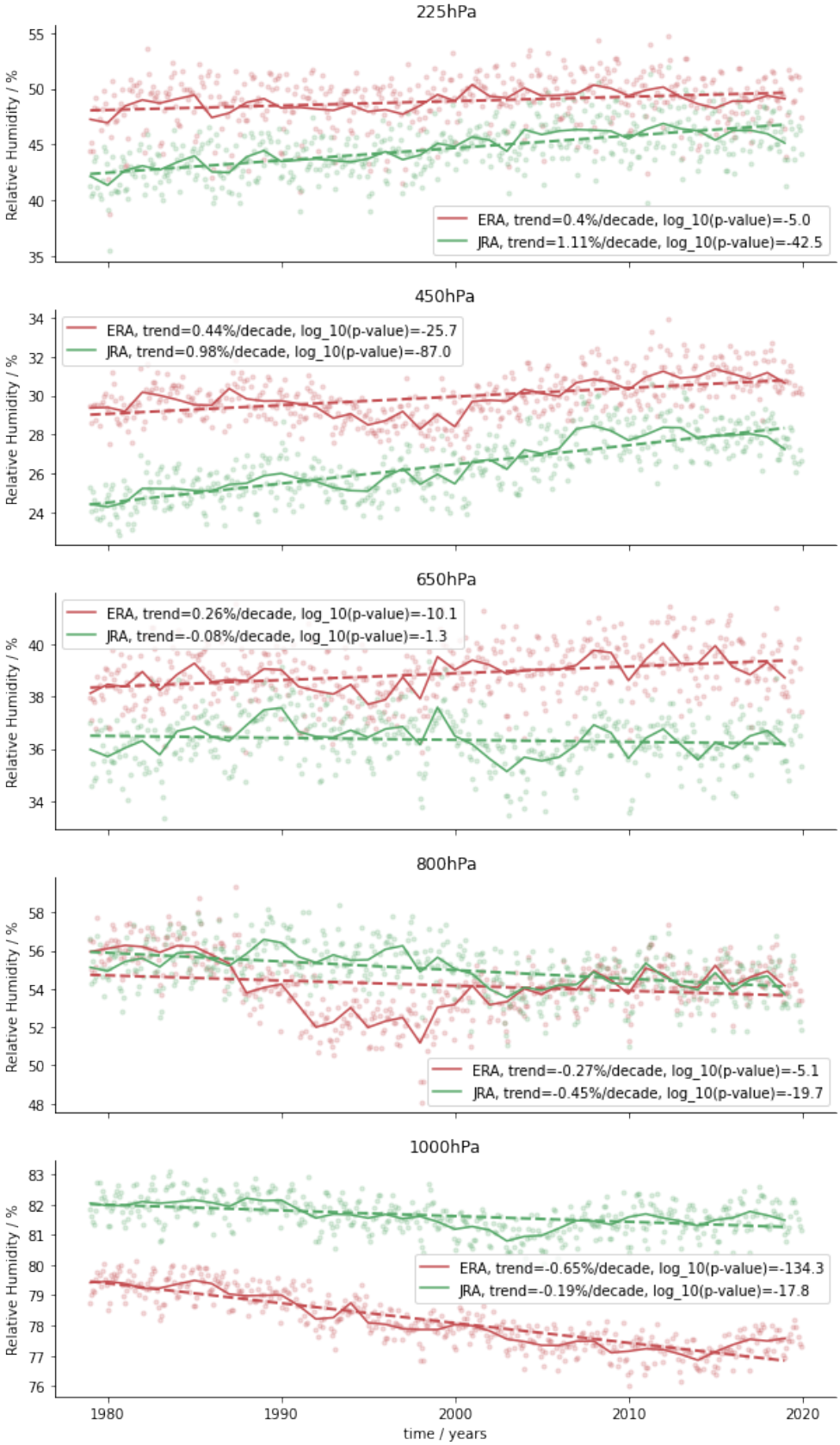
225hPa
Relative Humidity / %
ERA, trend=0.4%/decade, log_10(p-value)=-5.0
JRA, trend=1.11%/decade, log_10(p-value)=-42.5
450hPa
Relative Humidity / %
ERA, trend=0.44%/decade, log_10(p-value)=-25.7
JRA, trend=0.98%/decade, log_10(p-value)=-87.0
650hPa
Relative Humidity / %
ERA, trend=0.26%/decade, log_10(p-value)=-10.1
JRA, trend=-0.08%/decade, log_10(p-value)=-1.3
800hPa
Relative Humidity / %
ERA, trend=-0.27%/decade, log_10(p-value)=-5.1
JRA, trend=-0.45%/decade, log_10(p-value)=-19.7
1000hPa
Relative Humidity / %
ERA, trend=-0.65%/decade, log_10(p-value)=-134.3
JRA, trend=-0.19%/decade, log_10(p-value)=-17.8
1980
1990
2000
2010
2020
time / years

1.4 Decade differences

As an other way to check the robustness of the trend we observe here, we computed the differences for both datasets at each levels * between the last (2010-2019) and the first (1979-1988) decades * between the second-to-last (2000-2009) and the first decades. * between the last and the second (1989-1999) decade.

[10]:
```
[Plotting commands]

ax[0].plot((np.mean(H_trop_ERA[-120:],0) - np.mean(H_trop_ERA[:120],0))/3,␣
 ↪P_ERA, c= sns.color_palette("deep")[3])
ax[0].plot((np.mean(H_trop_JRA[-120:],0) - np.mean(H_trop_JRA[:120],0))/3,␣
 ↪P_JRA, c= sns.color_palette("deep")[2])
ax[1].plot((np.mean(H_trop_ERA[-240:-120],0) - np.mean(H_trop_ERA[:120],0))/2,␣
 ↪P_ERA, c= sns.color_palette("deep")[3])
ax[1].plot((np.mean(H_trop_JRA[-240:-120],0) - np.mean(H_trop_JRA[:120],0))/2,␣
 ↪P_JRA, c= sns.color_palette("deep")[2])
ax[2].plot((np.mean(H_trop_ERA[-120:],0) - np.mean(H_trop_ERA[120:240],0))/2,␣
 ↪P_ERA, c= sns.color_palette("deep")[3])
ax[2].plot((np.mean(H_trop_JRA[-120:],0) - np.mean(H_trop_JRA[120:240],0))/2,␣
 ↪P_JRA, c= sns.color_palette("deep")[2])

[...]
```

[10]:

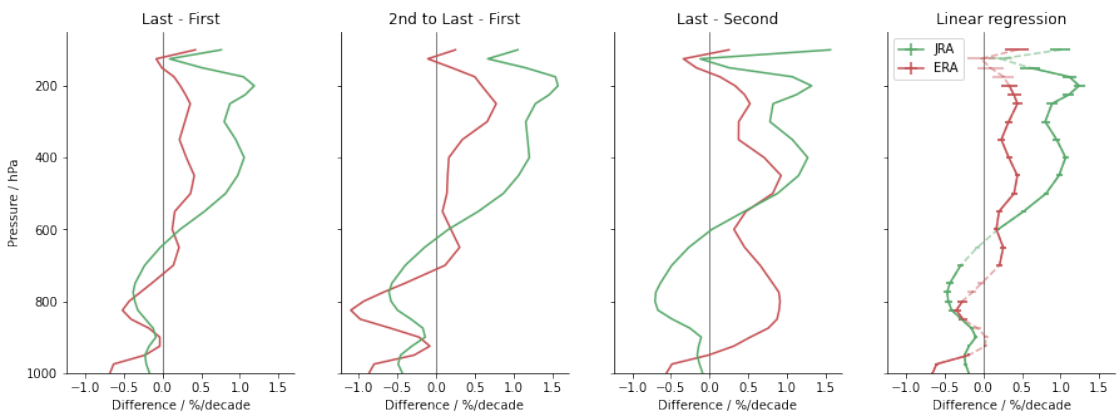

Most of it is coherent, except for one noticeable difference with the second decade of ERA, where we can see in the time series (for example at 800hPa) that relative humidity is lower during this period, for a reason we do not know.

2 Line-by-line analysis for Section 3

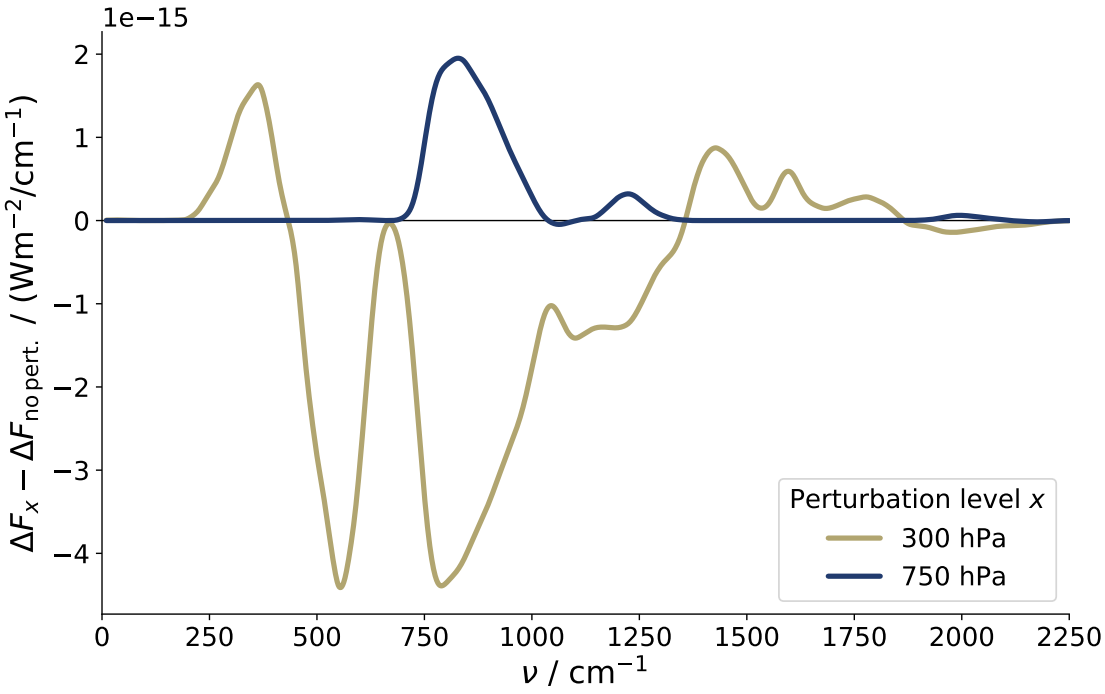

Figure S2. Difference in the "humidity forcing" for RH perturbations at different pressure heights.

Figure S2 shows the change in the "humidity forcing" for relative humidity RH perturbations at different pressure height. We define the humidity forcing as the difference in outgoing-longwave radiation (OLR) between an atmosphere in present-day conditions and an atmosphere in which the absolute humidity has been adjusted to a hypothetically 1-K-warmer temperature profile while preserving the actual temperature. This way, we can quantify the radiative forcing of the moistening of the atmosphere alone. The two lines in Figure S2 show how RH perturbations at different heights affect the humidity forcing: one can see that the change in OLR is increased in spectral regions close to the perturbation. We interpret this as an "anchoring effect" of the perturbation on the effecting emission height z_ϵ. For RH perturbations well above z_ϵ (300 hPa, yellowish line) a stronger increase of the emission height — a stronger forcing — in the atmospheric window overpowers this effect.

3 ECS for different uniform troposheric RH and different surface temperatures

In section 3 (§6) we write that decreasing T_0 reduces the sensitivity to RH.

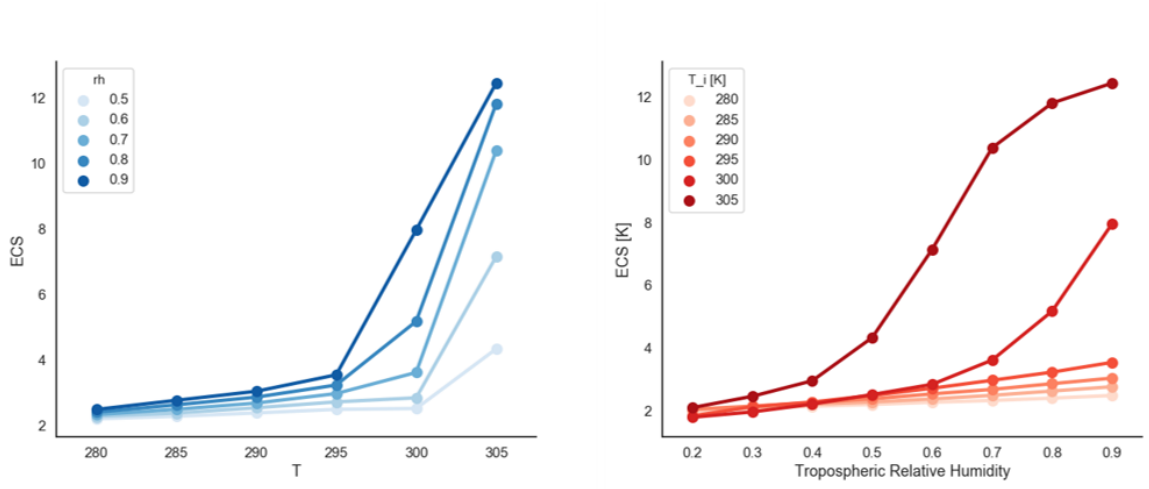

Figure S3. for a set of runs with different initial surface temperature T_0 and different uniform tropospheric RH. All were performed with a moist adiabatic Lapse Rate. Both plots display the same data, but on different axes.

The left panel of Fig. S3 shows this phenomenon. In general, because of the temperature–dependence effect,as highlighted by Meraner, Mauritsen, and Voigt 2013, the atmosphere is less sensitive for lowest temperature, as we can see in left panel of Fig. S3. This effect is even stronger in our case when using $T_0 \geq 300K$, because of the closing of the atmospheric window for such conditions.